Energy 220 (2021) 119680

Contents lists available at ScienceDirect

Energy

journal homepage: www.elsevier.com/locate/energy

Wind farm power maximization through wake steering with a new multiple wake model for prediction of turbulence intensity

Guo-Wei Qian, Takeshi Ishihara*

Department of Civil Engineering, School of Engineering, The University of Tokyo, 7-3-1 Hongo, Bunkyo-ku, Tokyo, 113-8656, Japan

ARTICLE INFO

Article history:
Received 5 August 2020
Received in revised form
29 November 2020
Accepted 18 December 2020
Available online 24 December 2020

Keywords:
Wake steering
Wind farm power maximization
Multiple wake model
Turbulence intensity
Lookup table
Yaw offset limit

ABSTRACT

A new multiple wake model is developed for wind farm power prediction and wind farm control. First, numerical simulations are conducted for two wind turbines under different layout sets, and the characteristics of mean velocity and turbulence intensity in multiple wakes are systematically investigated. A new multiple wake model considering the local effective turbulence on the rotor and the wake interaction effects is proposed. The proposed model can favorably predict the mean velocity and turbulence intensity distributions in multiple wake regions, as well as the power production in wind farm comparing with numerical simulations and field measurements. Finally, the new proposed multiple wake model is applied to wind farm modelling and optimization framework, which enables the maximization of wind farm power production by wake steering control. The wind sector width of 2° with the wind speed bin of 0.5 m/s is proposed for the lookup-table-based wake steering optimization. The proposed values reduce the prediction error of annual energy production gain from 34.5% to 3.2% comparing with the conventional values of 5° and 1 m/s. In addition, the yaw offset limit of ±15° is recommended to satisfy both the maximization of power production and the safety requirement of International Electrotechnical Commission (IEC) standard.

1. Introduction

In the wind farm, wakes from multiple turbines lead to a significant wake-turbine interaction as well as the wake-wake interaction, which reduces the whole energy output of the farm and also increase the turbulence intensity level inside the wind farm. The promise of wind farm control by coordinating the individual pitch or yaw control operations across the wind turbines to mitigate the wake losses has been studied around more than a decade [1]. The main objectives of wind farm control include increasing power production, reducing turbine loads, and providing electricity grid support services, while the increased energy production is seen as the most important benefit [2]. Moreover, in the report by Giebel et al. [3]; the yaw-based wake steering is shown to be the best option of wind farm control for Annual Energy Production (AEP) increase. As summarized by Kheirabadi and Nagamune [1], there are mainly the following aspects involved in the assessment of potential of yaw-based wake steering control: evaluation model, optimization method, inputs, wind conditions and relative efficiency gain, which are elaborated in detail as follows.

Firstly, to evaluate the potential of the wake steering control, several works have been extensively conducted by using parametric wake models [4–6]. To efficiently evaluate the wind farm power production under various wind conditions and turbine operation during the optimization process, the multiple wake effects are necessary to be modelled and the commonly used approach is to combine the single wake calculation based on the superposition approach for mean flow field [7–9]. More recently, a novel momentum-conserving wake superposition method is proposed by Zong and Porté-Agel [10];,however, the local turbulence intensity was not carefully considered in the multiple wake modelling. In the analytical modelling of wind farm by Niayifar and Porté-agel [8], the added turbulence from the nearest upstream turbine is solely considered for each wind turbine, while turbulence distribution is assumed to be top-hat with a wake diameter, which is questionable since the turbulence has been demonstrated to be dual-Gaussian distributed in a single wake region [11,12]. Note that the added turbulence intensity is an important feature for the wind farm flow field, which has a significant impact on the wake recovery and interactions, and thus increases both the variability in

* Corresponding author.
E-mail address: ishihara@bridge.t.u-tokyo.ac.jp (T. Ishihara).

https://doi.org/10.1016/j.energy.2020.119680
0360-5442/

power production and structural loads of the downstream turbines. Therefore, an accurate evaluation of turbulence variation in the multiple wake region is essential for proper wind farm power prediction and maximization.

As for the optimization method, various optimization algorithms like the centralized gradient-based programming are utilized in offline phases, including wake model based optimization studies [4–6], numerical simulations [13,14]. However, in the field implementation of wake steering control [15–17], considering the computational complexity, it is seldom to perform an online optimization of yaw offset based on the time series of measured wind conditions. Instead, the yaw offset angle for each turbine is pre-optimized for a set of wind conditions with certain bin widths for the wind speed and direction, generating a lookup table (LUT) with dimensions of turbine number, wind direction, wind speed, and turbulence intensity. Subsequently, an online LUT-based optimization is implemented, in which the optimal yaw offsets are obtained by interpolation based on the measured wind condition. The wind sector width of 5° and wind speed bin of 1 m/s is widely used to estimate AEP of wind farm considering the wake effects, which was accordingly adopted in the LUT-based optimization. However, since the wake steering control is highly sensitive to the wind direction and wind speed, whether the above conventional value is fine enough in engineering application should be answered and quantitatively evaluated by AEP gain.

The input used in the wake steering has universally been the yaw angle, where the maximum and minimum of allowed intentional yaw offset angles, i.e. yaw offset limits, were set to various values in the previous research [4–6]. Note that the maximum yaw misalignment of 15° is required by IEC standard for safety consideration [18], and a larger yaw offset would probably increase the fatigue load on wind turbine. Therefore, what a proper yaw offset limit should be utilized is of high importance, since it can avoid unnecessarily increased loads on turbines and ensure a satisfactory power gain at the same time. This study aims at proposing a new multiple wake model for prediction of turbulence intensity and then apply it to investigate the proper bin width of wind direction and yaw offset limit in the LUT-based wake steering optimization for wind farm power production.

In this study, the numerical model, setup, and the wake superposition method for mean velocity and turbulence intensity are presented in Section 2. Section 3 firstly illustrates the numerical results of wakes from two wind turbines. The predicted mean velocity and turbulence intensity as well as power production are then compared with numerical simulations and field measurements to examine the accuracy of the proposed model. Finally, the proposed multiple wake model is applied to a wind farm by the yaw-based optimization framework, and the optimal bin widths for the wind sector and wind speed as well as the yaw offset limit for the LUT-based wake steering optimization are proposed to satisfy both the maximization of power production and the safety requirement of IEC standard. The conclusions of this study are summarized in Section 4.

2. Methodology

The numerical model to investigate the characteristics of multiple wakes is firstly introduced in Section 2.1, where the turbulence model, wind turbine model and the numerical setup used in the numerical simulations are described. The single wake model, including rotor onset quantity, velocity deficit, added turbulence, and wake deflection, as well as the superposition principle of velocity deficit to formulate multiple wake model, are then presented in Section 2.2. Finally, the wind farm model for power prediction and its optimization framework based on wake steering control are described in Section 2.3.

2.1. Numerical model and setup

The Reynolds Stress turbulence Model (RSM) accounts for the anisotropic turbulence stresses to give accurate predictions for complex flows, which is an important advantage compared to the common two-equation Reynolds-averaged Navier–Stokes (RANS) models with isotropic eddy-viscosity hypothesis. Additionally, as pointed out by Cabezón et al. [19], the common two-equation RANS models like the standard $k-\varepsilon$ model could not provide good prediction for the wind turbine wakes, while RSM shows good performance for prediction of wind turbine wakes [20].

In this study, the RSM with Linear Pressure-Strain model in ANSYS Fluent 16.2 [21] is used to express the Reynolds stress tensor to close the momentum equation. Finite volume method is employed to perform the numerical simulation. The default values recommended by the Fluent Theory Guide [21] are used for all the model parameters. The second-order upwind scheme is applied for the interpolation of velocities, turbulent dispassion term, and Reynolds Stress. SIMPLE (semi-implicit pressure linked equations) algorithm is employed for solving the discretized equations [22].

A utility-scale wind turbine model is adopted to study the multiple wake characteristics. It is based on the offshore 2.4 MW wind turbine at the Choshi demonstration site with the rotor diameter of $D = 92.0$ m and the hub height of $H = 80.0$ m [11]. The effect of the rotor induced forces on the flow is parameterized by using an actuator disk model with rotation (ADM-R), in which the lift and drag forces are calculated based on the blade element theory [23] and then unevenly distributed on the actuator disk. The rotor can be rotated around the z-axis enabling to change the yaw angle of turbine. The nacelle and tower are modelled as a porous medium with a packing density of 99.9%. The details of the ADM-R model in RSM simulations were introduced in references [20], and its accuracy for wind turbine wake simulations was validated by the wind tunnel experiment.

This study firstly focuses on the simplest multiple wake configuration, where the two wind turbines are aligned with the mean wind direction as shown in Fig. 1. The computational domain has the streamwise length of 25D, the spanwise length of 10D, and the height of 3.2D. It is noted that the general numerical simulation settings including critical mesh size and fluid conditions in current study are exactly identical to those in reference [20]. The first upstream wind turbine is placed at the center in the spanwise direction, and 4D downstream the inlet. The main domain is divided by a set of rectangular cells using the commercial grid-generation software GAMBIT 2.4.6 [24]. The region around the rotors is uniformly divided with the spatial resolution of 0.05D, which denotes

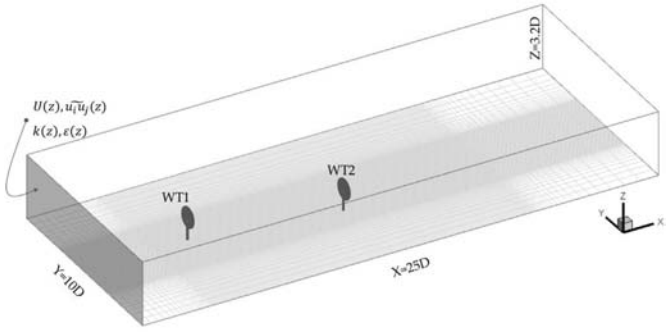

Fig. 1. Bird's eye view of the computational domain.

that there are at least 20 grid points covering the rotor diameter in the spanwise and vertical directions. The mesh is stretched horizontally away from the wake region towards the domain boundaries with a growth ratio of 1.15. The grid size starts from 0.0018D at the bottom and grows with a ratio of 1.1 in the vertical direction. A total number of cells is around 2.5 million. Boundary conditions used in the numerical simulations are summarized as follows: the values of $U(z)$ and $\overline{u_i u_j}(z)$ extracted from the LES simulations conducted for neutral atmospheric boundary layer with a hub height mean wind speed of 10 m/s and ambient turbulence intensity of $I_a = 0.035$ [11] are imposed at the inlet to represent the offshore ambient inflow; the inflow profile of $k(z)$ and $\varepsilon(z)$ are determined by assuming a local equilibrium of production and dissipation of turbulence kinetic energy $P_{ii} = 2\rho\varepsilon$ in the streamwise direction; a symmetry condition is used at the top and spanwise sides; an outflow condition is applied at the end of the domain; the wall-stress boundary condition is imposed at the ground surface based on the logarithmic law.

As shown in Fig. 2, two wind turbines with a distance of 7D under three wind directions of 0°, 5°, and 10° are chosen as three representative cases to simulate the multiple wakes: (a) In-line with full overlap, where the downstream wind turbine is wholly in the wake; (b) Partial offset ($\Delta y < D$) with partial overlap, where the downstream turbine is partially affected by the wake; (c) Fully offset ($\Delta y > D$) with partial overlap, where the turbine rotor is fully offset from the upstream rotor, but still partially disturbed by the expanded wake. In the cases (a) and (b), both wake-wake interaction and wake-turbine interaction effects exist, while in the case (c), the wake-wake interaction effect is dominant and the wake-turbine interaction effect is negligible. The parameters used in the numerical simulation for each case are summarized in Table 1, in which the thrust coefficient C_T of the upstream turbine is kept the same and C_T of the downstream one is determined by the rotor averaged wind speed as the relative location changes under different wind directions.

Table 1
Parameters used in numerical simulations.

Case	Wind direction	Longitudinal offset Δx	Lateral offset Δy	C_T	
				WT1	WT2
(a)	0°	7.000 D	0	0.36	0.70
(b)	5°	6.998 D	0.612 D	0.36	0.46
(c)	10°	6.893 D	1.234 D	0.36	0.38

2.2. Single wake model and superposition principle

Most single wake models take the assumption that a uniform flow enters the rotor plane, while it is not applicable to the real situation since the turbines inside the farm generally experience a non-uniform inflow due to the wakes from upstream turbines. Hence, to apply the wake models in a wind farm, the equivalent wind speed $U_{h,i}$ and turbulence intensity $I_{a,i}$ on the rotor, i.e., the rotor onset wind speed and turbulence intensity should be firstly evaluated. As shown in Equations (1) and (2), the rotor onset $U_{h,i}$ is calculated by directly performing a geometric averaging of wind speed U over the rotor, while rotor onset $I_{a,i}$ is calculated by the root mean of squares of streamwise turbulence standard deviation σ_u over the rotor divided by the rotor onset wind speed $U_{h,i}$.

$$U_{h,i} = \frac{1}{A}\int_{rotor} U(x_i, y, z)dA \tag{1}$$

$$I_{a,i} = \frac{1}{AU_{h,i}}\sqrt{\int_{rotor} \sigma_u^2(x_i, y, z)dA} \tag{2}$$

where x_i denotes the streamwise location of turbine, and A is the area of the rotor.

The Gaussian-based analytical single wake model proposed by Ishihara and Qian [11] and Qian and Ishihara [20], noted as Ishihara-Qian model, provides a three-dimensional wake characteristic including wake width, velocity deficit, added turbulence, as well as wake deflection caused by yaw offset. In Ishihara-Qian model, all the parameters are automatically determined as the function of ambient turbulence intensity and thrust coefficient. Moreover, this wake model firstly provided the double-Gaussian distribution for turbulence intensity in the wake region. Also, as recently reported by Brugger et al. [25]; among three conventional analytical wake models, the Ishihara-Qian model gave the smallest errors compared to the SCADA data and the power estimated from the Doppler Lidar measurements. Therefore, the Ishihara-Qian model is utilized in this study for multiple wake modelling. The detailed formula and parameters of the single wake model are summarized in Table 2, where the rotor onset wind speed $U_{h,i}$ and turbulence intensity $I_{a,i}$ will be used to replace the U_h and I_a of ambient wind condition for multiple wake prediction. Note that the minimum I_a in the Ishihara-Qian model is 0.03 and should be used for the cases when the ambient turbulence intensity is lower than 0.03.

To predict the mean flow field U at a given position in the multiple wake region, there are four kinds of superposition methods commonly used in the literature [10,26], which are categorized as shown in Table 3. Here, U_0 is the free stream wind speed, ΔU_i is the single wake velocity deficit induced by wind turbine WTi in stand-alone conditions. The differences among these methods depend on the two issues: (1) the approach of defining the single wake deficit ΔU_i, where it is calculated with respect to the free-stream velocity of $U_{h,0}$ in the Ambient-based definition, while with

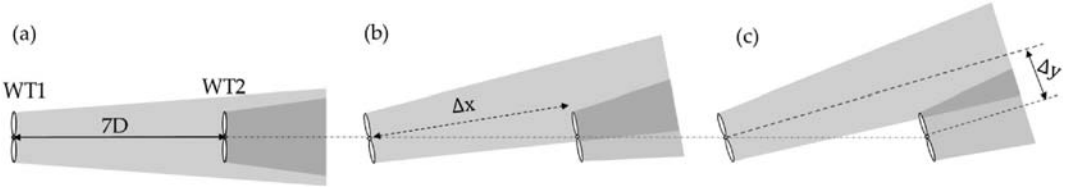

Fig. 2. Wind turbine layouts under different wind directions: (a) In-line with full overlap: wind direction of 0°; (b) Partial offset with partial overlap: wind direction of 5°; (c) Fully offset with partial overlap: wind direction of 10°. D is the diameter of wind turbine rotor. Δx and Δy are the longitudinal distance and lateral offset, respectively.

Table 2
Summary of the Ishihara-Qian model

Wake model	Formulas	Parameters
Wake width	$\frac{\sigma}{D} = k^*\frac{x}{D} + \varepsilon^*$, $D_w = 4\sqrt{2ln2}\sigma$	$k^* = 0.11C_T'^{1.07}I_a^{0.20}$ $\varepsilon^* = 0.23C_T'^{-0.25}I_a^{0.17}$
Velocity deficit	$\Delta U(x,y,z)/U_h = \frac{1}{\{a + b\cdot x/D + c(1+x/D)^{-2}\}^2}\cdot\exp\left(-\frac{r^2}{2\sigma^2}\right)$ $r = \sqrt{(y-y_d)^2 + (z-H)^2}$	$C_T' = C_T(U_h,\gamma)\cos\gamma$, $I_a \geq 0.03$ $a = 0.93C_T'^{-0.75}I_a^{0.17}$ $b = 0.42C_T'^{0.6}I_a^{0.2}$ $c = 0.15C_T'^{-0.25}I_a^{-0.7}$
Added turbulence	$\Delta\sigma_u(x,y,z)/U_h = \frac{1}{d + e\cdot x/D + f(1+x/D)^{-2}}\left\{k_1\exp\left(-\frac{(r-D/2)^2}{2\sigma^2}\right) + k_2\exp\left(-\frac{(r+D/2)^2}{2\sigma^2}\right)\right\} - \Delta I_a$ $\Delta I_a = \begin{cases} 0 & else \\ I_a\sin^2\left(\pi\frac{H-z}{D}\right)\cos^2\left(\pi\frac{y}{D}\right) & (0 \leq z < H, \lvert y\rvert \leq D) \end{cases}$	$d = 2.3C_T'^{-1.2}$, $e = 1.0I_a^{0.1}$ $f = 0.7C_T'^{-3.2}I_a^{-0.45}$ $k_1 = \begin{cases} cos^2(\pi/2\cdot(r/D-0.5)) & r/D \leq 0.5 \\ 1 & r/D > 0.5 \end{cases}$ $k_2 = \begin{cases} cos^2(\pi/2\cdot(r/D+0.5)) & r/D \leq 0.5 \\ 0 & r/D > 0.5 \end{cases}$
Deflection	$\frac{y_d(x)}{D} = \begin{cases} \theta_0\frac{x}{D} & (x \leq x_0) \\ \frac{\sqrt{C_T'}sin\gamma}{18.24k^*cos\gamma}ln\left\lvert\frac{(\sigma_0/D + 0.21\sqrt{C_T'})(\sigma/D - 0.21\sqrt{C_T'})}{(\sigma_0/D - 0.21\sqrt{C_T'})(\sigma/D + 0.21\sqrt{C_T'})}\right\rvert + \theta_0\frac{x_0}{D} & (x > x_0) \end{cases}$	$\theta_0 = \frac{0.3\gamma}{\cos\gamma}(1 - \sqrt{1-C_T'})$ $\frac{\sigma_0}{D} = \sqrt{C_T'\left(\frac{sin\gamma}{44.4\theta_0 cos\gamma} + 0.042\right)}$ $\frac{x_0}{D} = \frac{\sigma_0/D - \varepsilon^*}{k^*}$

Table 3
Summary of wake superposition methods used to calculate the mean velocity in multiple wakes.

Wake Superposition method	Superposition principle	Single wake deficit definition
Ambient-based Linear Sum [9]	$U = U_0 - \sum_{i=1}^{n}\Delta U_i$	$\Delta U_i = U_{h,0}(1 - U_i/U_{h,0})$
Rotor-based Linear Sum [8]	$U = U_0 - \sum_{i=1}^{n}\Delta U_i$	$\Delta U_i = U_{h,i}(1 - U_i/U_{h,i})$
Ambient-based Root Sum Square [7]	$U = U_0 - \sqrt{\sum_{i=1}^{n}\Delta U_i^2}$	$\Delta U_i = U_{h,0}(1 - U_i/U_{h,0})$
Rotor-based Root Sum Square [35]	$U = U_0 - \sqrt{\sum_{i=1}^{n}\Delta U_i^2}$	$\Delta U_i = U_{h,i}(1 - U_i/U_{h,i})$

respect to the local speed of $U_{h,i}$ experienced by turbines in the Rotor-based case; (2) the principle adopted to combine the velocity deficit from upstream turbines whose wakes affect the flow in that location, which includes linear sum and root sum square. In the Ambient-based method as shown in Appendix A, the mean wind speed velocity perceived by the downstream turbines is substituted by the freestream wind speed during the single wake calculations, i.e. $U_{h,i} = U_{h,0}$, which neglected the wake interaction effects and can only applicable in the cases of very large turbine spacing. To overcome this drawback, instead of using the freestream wind speed, the local wind speeds experienced by wind turbines are determined consecutively from upwind to downwind in the Rotor-based method. The difference between superposition principle is also briefly explained here. In the Linear Sum method, the wake velocity deficits induced by all upstream turbines are summed linearly to conserve the total momentum deficit in the wake. However, in the Root Sum Square method, the velocity deficit in the multiple wakes is calculated by summing the squares of the individual velocity deficits. As investigated by Niayifar and Porté-Agel [8]; the generally linearized momentum deficit can be conserved by applying the linear superposition of velocity deficit, and the Rotor-based definition can provide more reasonable predictions compared with that by the Ambient-based definition. Therefore, in this study, individual velocity deficits are combined by utilizing the Rotor-based Linear Sum as

$$U = U_0 - \sum_{i=1}^{n}(\Delta U_i) \tag{3}$$

$$\Delta U_i / U_{h,i} = F(C_{T,i}, I_{a,i}, (x - x_i)/D)\varphi(r_i/\sigma_i) \tag{4}$$

where U_0 is the free stream wind speed, ΔU_i is the velocity deficit induced by wind turbine WTi and calculated by the Ishihara-Qian model, F and φ is the streamwise function and spanwise function (see Table 2), respectively, $C_{T,i}$ is the thrust coefficient of turbine WTi, σ_i is the representative wake width, r_i is the spanwise distance from the wake center, D is the rotor diameter.

2.3. Wind farm power maximization framework by wake steering control

A wind farm power maximization framework, incorporating the ambient wind condition, turbine model, wake model, and optimizer, is designed to achieve the maximum power by wake steering control. As shown in Fig. 3, the wind speed, wind direction, and turbulence intensity of ambient inflow are firstly inputted to initialize the flow field. The rotor onset quantity of each wind turbine is then updated from upstream to downstream and simultaneously result in the wake flow field in the wind farm through the wake model calculation. The wind turbine model is a feedback loop

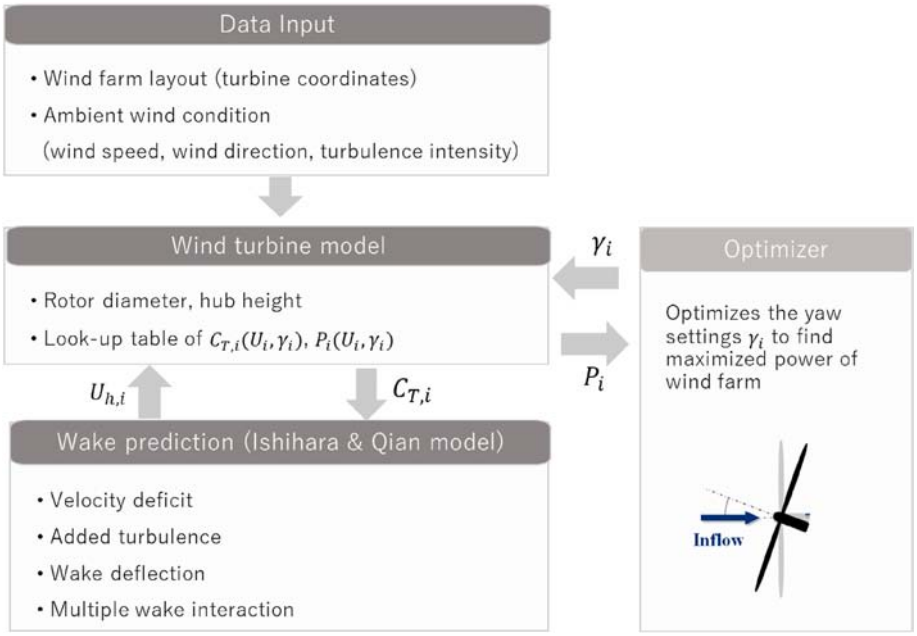

Fig. 3. Schematic overview of the wind farm power maximization framework by wake steering control.

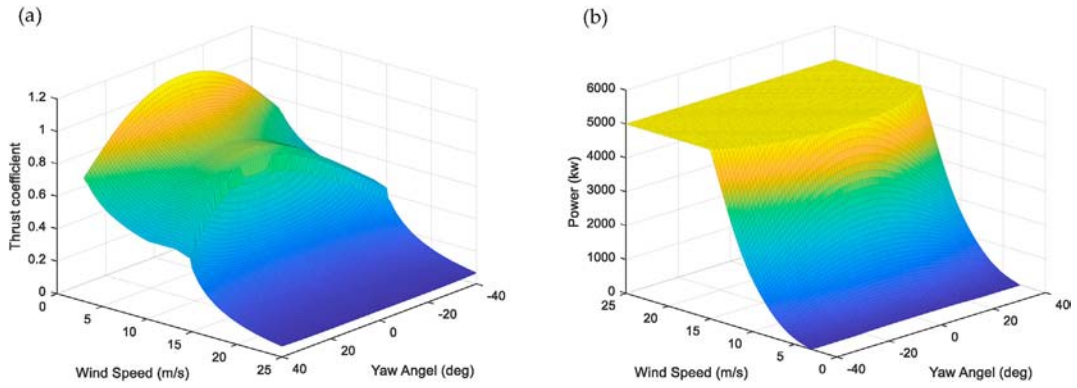

Fig. 4. Thrust coefficient (a) and power curve (b) of the NREL 5-MW reference wind turbine as a function of wind speed U and yaw angle γ.

with the wake, where the turbine operation condition and power are determined by the rotor onset wind speed, and the resulted thrust coefficient determines the wake flow and onset values of downstream turbines.

In this study, the NREL 5-MW reference wind turbine model is used to provide detailed information on the wind turbine model. It has a rotor diameter of $D = 126.0$ m, and a hub height of H = 90.0 m. Following the approach recommended by Gebraad [5], the wind turbine model is represented by a two-dimensional lookup table of thrust coefficients $C_T(U_h,\gamma)$ and power curves $P(U_h,\gamma)$ as shown in Fig. 4, in which the thrust coefficients and power curves under different wind speeds and yaw offsets are pre-calculated by FAST [27], where the thrust coefficient is defined as $C_T(U_h,\gamma) = F_T(U_h,\gamma)/\left(0.5\rho A U_h^2\right)$. During the wind farm simulations, the rotor operation condition is evaluated through the interpolation of these pre-calculated database. The wake models presented in Section 2.2 and Section 3.2 are utilized to calculate the wake effects. The power obtained from the wind farm model is transmitted to an optimizer to optimize the yaw offset γ_i of each wind turbine to find the maximized power production of the wind farm.

This study focuses on maximizing power output of wind farm at a site with a given wind condition, using the set-points for the yaw angels of the turbines as the optimization variable. As formulated in Equation (5), the optimization problem aims at finding the set of optimal yaw offset angles $\boldsymbol{\gamma}^{\text{opt}}(\theta,U,I_a) = \{\gamma_1^{\text{opt}}\ldots,\gamma_i,\ldots\gamma_{N_T}^{\text{opt}}\}$ for N_T wind turbines, which maximizes the power output of the wind farm for the prescribed wind speed U, ambient turbulence intensity I_a and wind direction θ. The $(\gamma_{min},\gamma_{max})$ is the range of allowed yaw angle, i.e., yaw offset limit, and wind sector width as well as the values used in the previous researches are summarized in Table 4. The determination of yaw offset limit and wind sector width will be discussed in Section 3.3.

$$\boldsymbol{\gamma}^{opt}(\theta, U, I_a) = \underset{\gamma}{argmax} \sum_{i=1}^{N_T} P_i(\gamma_1, \ldots \gamma_i, \theta, U, I_a) \text{ Subject to } \gamma_{min} < \gamma_i < \gamma_{max} \quad (5)$$

To reliably handle optimization problem of larger numbers of design variables with a fast convergence, fmincon solver in MATLAB, a gradient-based optimization algorithm to find minimum of nonlinear problems with constraints, is adopted in this study. Besides, to guarantee the local minima found by fmincon are in fact global minima, MATLAB's Global Search solver is used. Simply put, the Global Search algorithm generates a number of test points to use as initial starting points for the fmincon solver. As the algorithm steps through the list of test points, it discards any that is found to be in existing basin. At the end, it reports the local minimum with the smallest cost function among the solutions calculated from the test points. The details of solver can be found in the MATLAB documentation [28].

It is noted that the optimal yaw offset is strongly dependent on the wind direction since it determines the relative location between the wake and downstream turbines affected. In this study, the performance of LUT-based optimization with different bin width of wind direction is evaluated with the comparison to real-time optimization. As illustrated in Fig. 5, the time series data of measurements consisting of 10-min average wind speed $\overline{U}_{10\text{min}}(t)$ and wind direction $\overline{\theta}_{10\text{min}}(t)$ are taken as the input to the LUT of yaw offsets and Gradient-based optimizer to find a set of optimal yaw offset angle $\boldsymbol{\gamma}_{LUT}^{opt}(t)$ and $\boldsymbol{\gamma}_{RT}^{opt}(t)$, based on which the optimized power $\boldsymbol{P}_{LUT}^{opt}(t)$ and $\boldsymbol{P}_{RT}^{opt}(t)$ are obtained through the Ishihara-Qian model. The simulation of greedy yaw control is also performed to provide the baseline power output $\boldsymbol{P}^{greedy}(t)$, where all the turbines is yawing into the incoming wind direction without any intentional yaw offset. Finally, AEP gains, with respect to the power output of greedy yaw control, are calculated for the LUT-based and real-time optimizers, respectively.

3. Results and discussion

The mean velocity and turbulence intensity in the multiple wake region of two wind turbines with different wind directions are investigated by numerical simulations in Section 3.1. A new multiple wake model for turbulence intensity is then proposed. The mean velocity and turbulence intensity predicted by the proposed model are compared with those obtained from the numerical simulations and filed measurement in Section 3.2. Finally, wake steering optimization is conducted using the proposed multiple wake model. The optimal wind sector width, wind speed bin, and yaw offset limit for LUT-based wake steering are proposed in Section 3.3.

3.1. Multiple wake characteristics

In Fig. 6, the contours and profiles of simulated mean velocity in the wake region under different wind directions are firstly presented in the horizontal x-y plane at the hub height (z = H). The origin of the domain is set at the center of the downstream rotor (WT2). The mean velocities are normalized by the ambient free-stream wind speed $U_{h,0}$ at the hub height. The mean velocity profiles at the x = 4D downstream WT2 are extracted and shown in Fig. 6. The dashed lines mark the intersected wake region based on the individual wake boundary from two turbines, where the wake boundary is denoted by the positions with the mean velocity equal to the 95% of the free-stream velocity.

Table 4
Summary of yaw offset limit and wind sector width used in wake steering control.

Literature	Evaluation model	Yaw offset limit	Wind sector width
Gebraad et al. [13]	FLORIS, SOWFA, Real-time	0° ~ 40°	–
Fleming et al. [4]	FLORIS, Real-time	−10° ~ 25°	–
Gebraad et al. [5]	FLORIS, LUT-based	–	5°
van Dijk et al. [6]	FLORIS, LUT-based	−40° ~ 40°	5°
Munters and Meyers [14]	LES, Real-time	−30° ~ 30°	–

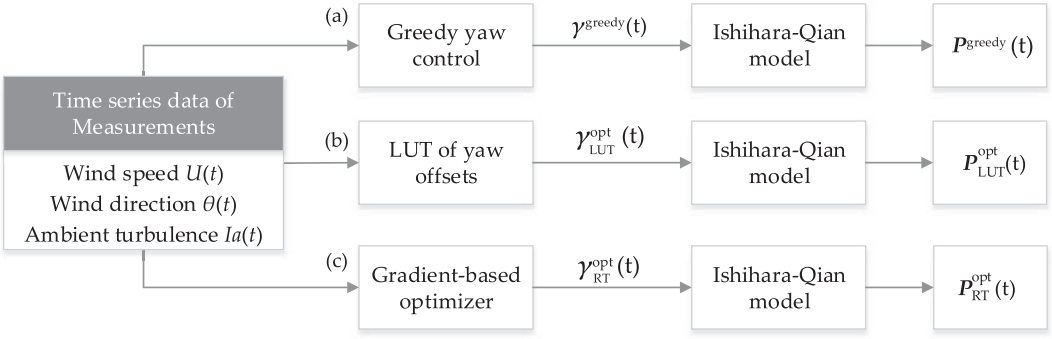

Fig. 5. Comparison between (a) greedy yaw control, (b) LUT-based optimization and (c) real-time optimization.

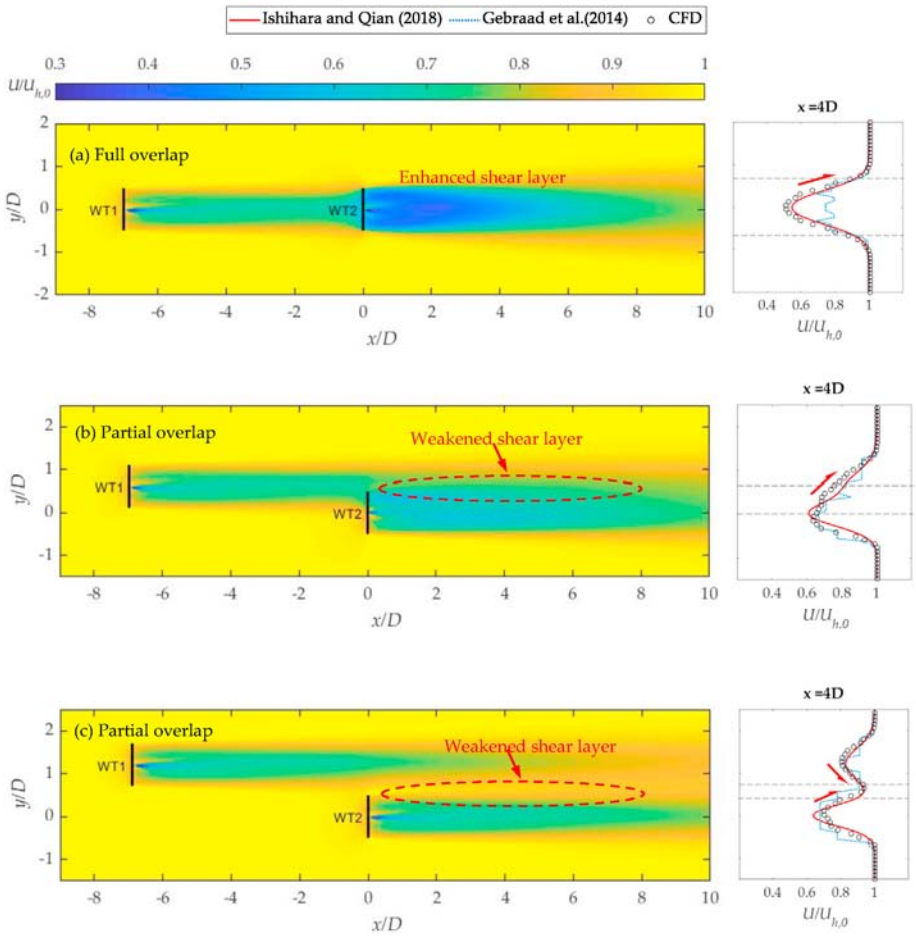

Fig. 6. Contours and profiles of mean velocity in the wake of two wind turbines: (a), (b), and (c) are results under wind direction of 0°, 5° and 10°, respectively. The wind turbines are presented by the solid black lines. The dashed lines mark the interaction region in the wakes of two turbines and the red rows denote the slope of velocity profiles in the horizontal direction. (For interpretation of the references to colour in this figure legend, the reader is referred to the Web version of this article.)

For the full overlap wakes of in-line layout (Fig. 6a), the rotor onset wind speed of WT2 becomes lower, which gives a larger thrust coefficient and stronger velocity deficits. As a result, the wake shear is enhanced with a steep slope in the intersected wake region. For partial offset layout case (Fig. 6b), the wake of downstream turbine WT2 is partially merged in the wake from WT1, thus the lateral slope of velocity in the side intersected with the upstream wake becomes gentler compared with the other side in free stream. Under the wind direction of 10° (Fig. 6c), though WT2 is fully offset from the upstream rotor WT1, its wake is still partially interacted with the wake from WT1. It can be found that, in the intersection area, the slope of velocity from two wakes are opposite, which also will weaken the wake shear layer as the wakes expand and propagate in the downstream. It is noted that since the added turbulence intensity in the wake region is mainly resulted from the velocity shear layer, this characteristic will be explained in the following discussion about turbulence intensity.

The mean velocity profiles predicted by wake models are also plotted in Fig. 6 to illustrate the quantitative comparison with numerical simulation results, where blue dashed lines are results predicted by the conventional multi-zone model with Ambient-based Root Sum Square superposition method proposed in FLORIS [13], and red solid lines represent the results calculated by the Ishihara-Qian model [11] based on the principle of Rotor-based Linear Sum with effective rotor onset. It can be seen that the Ishihara-Qian model generally presents favorable agreement with numerical results, while the conventional model underestimates the wake deficits in the full overlap region.

Fig. 7 shows contours and profiles of turbulence intensity in the horizontal x-y plane at the hub height. The turbulence intensity is defined as

$$I_u = \frac{\sigma_u}{U_{h,0}} \tag{6}$$

where σ_u is the streamwise turbulence standard deviation. The horizontal profiles of turbulence intensity at the x = 4D downstream the WT2 are extracted and shown in open circles. The results by directly combining wakes of two turbines, i.e. $\sqrt{\Delta I_{u,1}^2 + \Delta I_{u,2}^2}$, are also shown in blue lines in which $\Delta I_{u,1}$ and $\Delta I_{u,2}$ are added turbulence intensity predicted by Ishihara -Qian model for WT1 and WT2, respectively. Red solid lines present the results predicted by the new multiple wake model.

For the full overlap wakes shown in Fig. 7a, the turbulence intensity is generally characterized by a dual-peak both in the single wake region and the full overlap region. It can be found that the turbulence intensity in the center part, i.e. the interaction region, is increased, which is due to the enhanced velocity shear as discussed in Fig. 6a. For partial overlap cases under wind direction of 5° and 10° as shown in Fig. 7b and c, the contours and profiles demonstrate that the original peaks of turbulence intensity from the rotor tip side are flattened in the intersection wake region. This is also

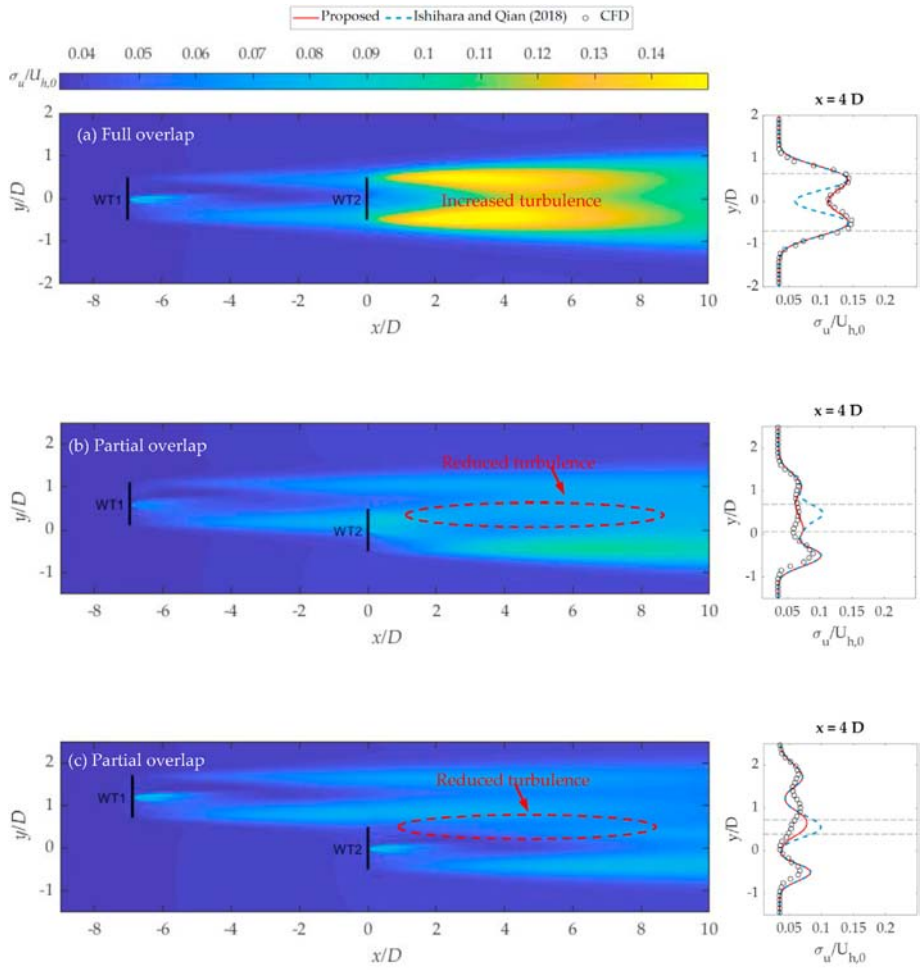

Fig. 7. Contours and profiles of turbulence intensity in the wake of two wind turbines: (a), (b), and (c) are results under wind direction of 0°, 5° and 10°, respectively. The wind turbines are presented by the solid black lines. The dashed lines mark the interaction region in wakes of two turbines. Blue solid lines show the results by directly combining added turbulence intensity individually predicted by Ishihara-Qian model for WT1 and WT2, respectively. Red solid lines present the results predicted by the new multiple wake model. (For interpretation of the references to colour in this figure legend, the reader is referred to the Web version of this article.)

related to the weakened velocity shear layer in the overlapped region as illustrated in Fig. 6b and c. To address the failure of the conventional approach in the wake interaction region, a new multiple wake model is proposed, which provides better performance as shown by the red solid lines in Fig. 7, and will be discussed in Section 3.2.

3.2. A new multiple wake model and its validation

In the IEC61400-1 for wind turbine design [18], the turbulence intensity in a wind turbine wake is estimated as

$$\sigma_u^2 = \sigma_{u,0}^2 + \Delta\sigma_u^2 \tag{7}$$

$$\Delta\sigma_u = \frac{1}{1.5 + \frac{0.8}{C_T}\frac{x}{D}} \tag{8}$$

where σ_u is the turbulence standard deviation in the wake region, $\sigma_{u,0}$ is the ambient turbulence standard deviation, and $\Delta\sigma_u$ is the turbulence standard deviation generated by the turbine. However, to the best of the authors' knowledge, no specific superposition principle has been reported yet for turbulence intensity in multiple wakes. In this study, Equation (7) used in the IEC61400-1 [18] is extended to formulate the turbulence intensity in the multiple wake region based on the principle of Linear Sum of Square (LSS) as

$$\sigma_u^2 = \sigma_{u,0}^2 + \sum_{i=1}^{n} \Delta\sigma_{u,i}^2 \tag{9}$$

where $\Delta\sigma_{u,i}$ is the individual added turbulence from the wind turbine WT*i*.

As discussed in Section 3.1, directly superposing the individual added turbulence intensity from two turbines by the principle of LSS is not availing, and therefore an additional correction term $\Delta\sigma_{u,ij}$ for the turbine WT*i* in a wind farm is proposed to consider the effects of wake interaction with its closest upstream turbine WT*j*. To this end, the LLS principle in Equation (9) is updated as

$$\sigma_u^2 = \sigma_{u,0}^2 + \sum_{i=1}^{n} \left(\Delta\sigma_{u,i} + \Delta\sigma_{u,ij}\right)^2 \tag{10}$$

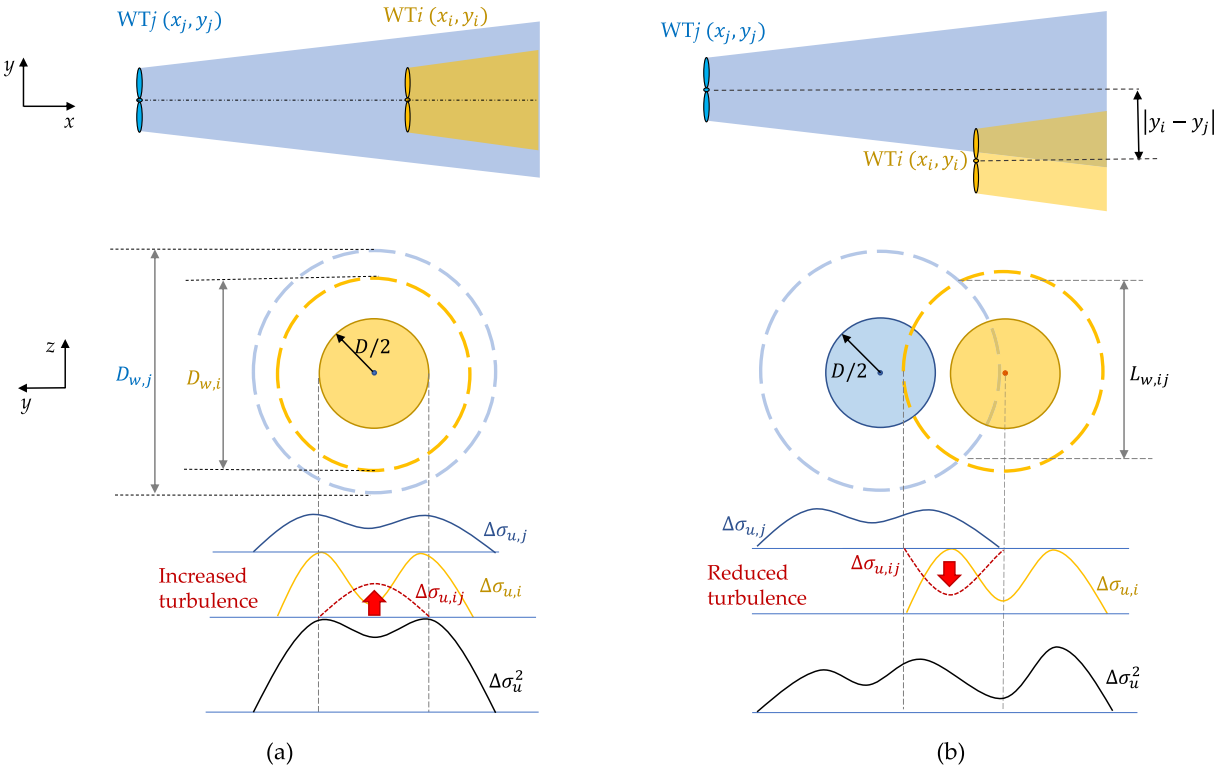

Fig. 8. Schematic of multiple wakes of turbulence intensity considering the wake interaction effects for (a) full overlap and (b) partial overlap wakes.

$$A_{P,1} = \left\{ (x_i, y_i) \middle| 0 < x_i - x_j < 15D,\ \frac{D_{w,j}(x_i) - D}{2} < \left| y_i - y_j \right| \le \frac{D_{w,j}(x_i) + D}{2} \right\},\ \textit{for partial overlap} \tag{13}$$

$$\Delta\sigma_{u,i} / U_{h,i} = G(C_{T,i}, I_{a,i}, (x - x_i) / D)\varphi(r_i / \sigma_i) \tag{11}$$

where the individual added turbulence from WT*i*, $\Delta\sigma_{u,i}$ is estimated by the Ishihara-Qian model, G and ϕ is the streamwise function and spanwise function, respectively (see Table 2).

The new multiple wake model is shown schematically in Fig. 8, in which the yellow and blue solid profiles denote the added turbulence standard deviation from the target turbine WT*i* and its closest upstream turbine WT*j*. The red dashed profiles represent the induced turbulence standard deviation by the turbulent mixing, which increases turbulence at the center of full overlap wake and decreases turbulence of partial overlap wakes in the wake interaction region. The black solid lines denote the finally resulted turbulence profiles.

Firstly, the full overlap and partial overlap wakes are defined for the target turbine WT*i* based on its relative position with respect to the position of the closest upstream turbine WT*j* as

where (x_i, y_i) and (x_j, y_j) are coordinates of the rotor center for target wind turbine WT*i* and its closest upstream turbine WT*j*, $D_{w,j}(x_i)$ is the wake width of WT*j* at the position of WT*i*. Here, the wake interaction effect is neglected if the streamwise distance between WT*i* and WT*j* is over 15D. Besides, the horizontal coordinate y_j needs to be modified to $(y_j + y_{d,j})$ to consider the wake deflection when wake steering control is implemented.

Secondly, the range of the wake interaction region where the proposed correction term works is defined in Equations (14) and (15). For full overlap case, the rotor areas of WT*i* is assumed to be considered for correction. For partial overlap case, the wake region of WT*i* intersected with that of WT*j* is corrected.

$$A_{F,2} = \left\{ (y, z) \middle| r_i \le \frac{D}{2} \right\},\ \textit{for full overlap} \tag{14}$$

$$A_{F,1} = \left\{ (x_i, y_i) \middle| 0 < x_i - x_j < 15D,\ \left| y_i - y_j \right| \le \frac{D_{w,j}(x_i) - D}{2} \right\},\ \textit{for full overlap} \tag{12}$$

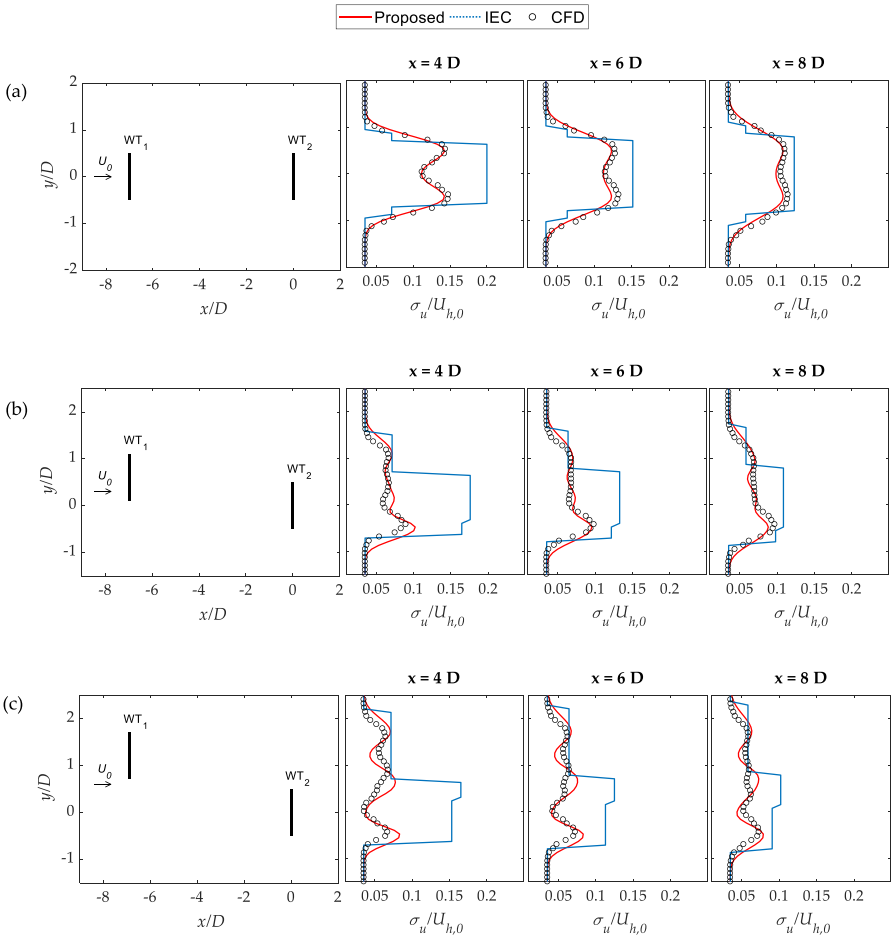

Fig. 9. Profiles of streamwise turbulence intensity in the wake of two wind turbines: (a), (b), and (c) are results under wind directions of 0°, 5° and 10°, respectively.

Table 5
Normalized Root Mean Square Error (RMSE) of predicted turbulence intensity with respect to numerical results in Fig. 9.

Model	Full overlap Wind direction = 0°	Partial overlap Wind direction = 5°	Partial overlap Wind direction = 10°
IEC61400-1	0.90	1.04	1.01
Proposed model	0.15	0.23	0.27

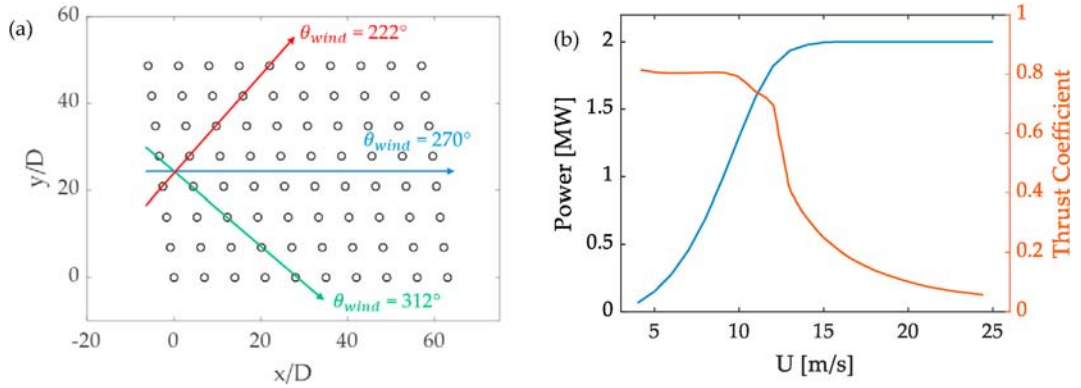

Fig. 10. Description of the Horns Rev wind farm: (a) schematic of layout and (b) power curve and thrust coefficient curve of Vestas V-80 2 MW wind turbine.

$$A_{P,2}=\left\{(y,z)\middle||y-y_i|<\frac{D_{w,i}}{2},|z-H|\le\frac{L_{w,ij}}{2},\mathrm{sgn}(y-y_i)\mathrm{sgn}\left(y_j-y_i\right)=1\right\},\ \textit{for partial overlap} \tag{15}$$

where r_i is the spanwise distance from the wake center of WT*i*, and $L_{w,ij}$ is the vertical length of the intersected wake region of WT*i* and WT*j*. They can be geometrically derived as

$$r_i=\sqrt{(y-y_i)^2+(z-H)^2} \tag{16}$$

$$L_{w,ij}=\frac{1}{\left|y_i-y_j\right|}\sqrt{\left(y_i-y_j\right)^2D_{w,j}^2-\left(\left(y_i-y_j\right)^2-D_{w,i}^2/4+D_{w,j}^2/4\right)^2} \tag{17}$$

Finally, the value of correction term is determined, which is assumed to be half of the added turbulence deviation at the tip side $\Delta\sigma_{u,i,tip}$, and then to be smoothed to the boundary of correction areas by using a cosine-like function as shown in Equation (18).

$$\Delta\sigma_{u,ij}=\begin{cases}\frac{1}{2}\Delta\sigma_{u,i,tip}\cos^2\left(\frac{\pi r_i}{D}\right) & ((x_i,y_i)\in A_{F,1},(y,z)\in A_{F,2},)\\ -\frac{1}{2}\Delta\sigma_{u,i,tip}\sin^2\left(\frac{\pi(y-y_i)}{D_{w,i}}\right)\cos^2\left(\frac{\pi(z-H)}{L_{w,ij}}\right) & ((x_i,y_i)\in A_{P,1},(y,z)\in A_{P,2})\\ 0 & else\end{cases} \tag{18}$$

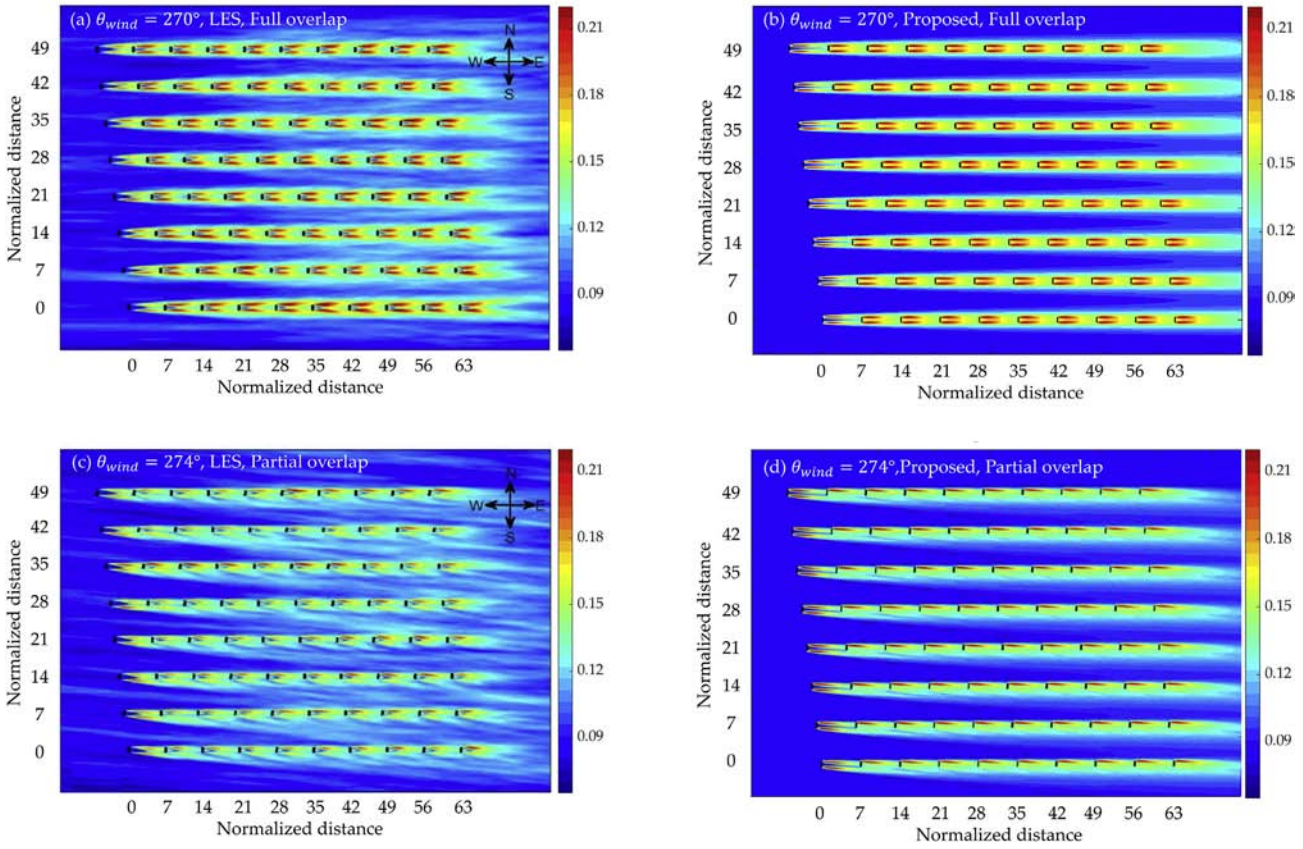

Fig. 11. Contours of streamwise turbulence intensity on a horizontal plane at the hub height for Horns Rec offshore wind farm under the freestream wind speed of 8 m/s: (a) and (c) are LES results [29]; (b) and (d) are results predicted by the proposed multiple wake model.

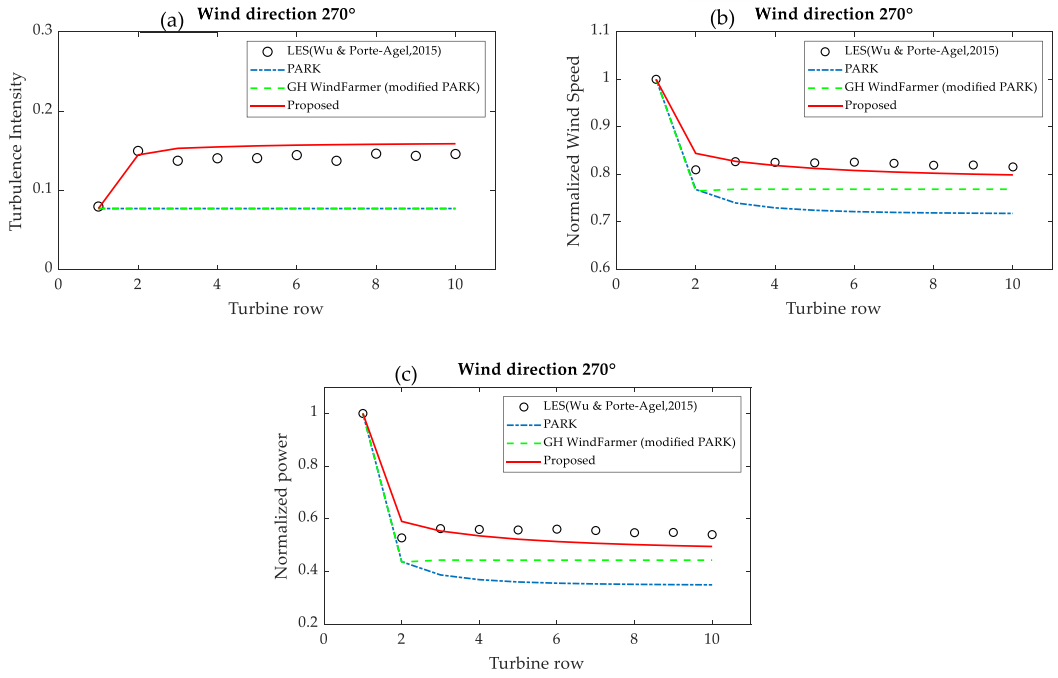

Fig. 12. Quantitative comparison of (a) the streamwise turbulence intensity at the hub height, (b) normalized mean wind speed incident on rotor, and (c) normalized mean power of each turbine under the wind direction of 270°. The mean velocity of LES is calculated based on the power curve and the corresponding power estimated by Wu and Porté-Agel [29].

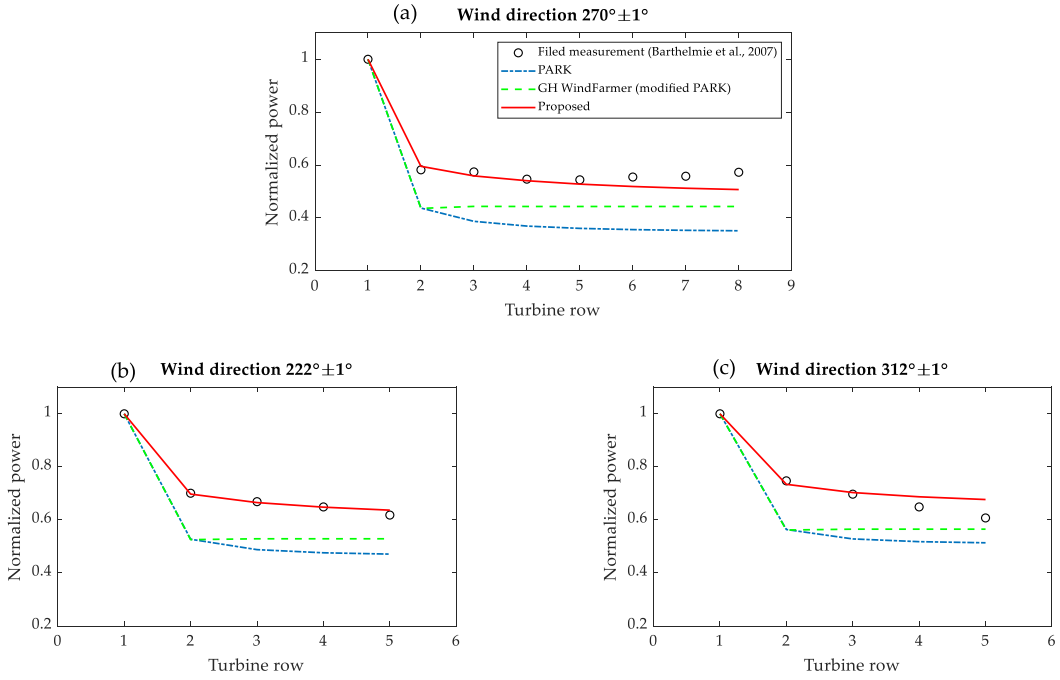

Fig. 13. Quantitative comparison of normalized power obtained from filed observations [30] and predictions by the PARK model, GH WindFarmer and the proposed multiple wake model: (a), (b), and (c) are results under wind direction of 270°, 222° and 312° with sector width of 2°, respectively. The freestream wind speed is 8 ± 0.5 m/s.

Fig. 9 shows the turbulence intensity profiles at selected positions at x = 4D, 6D and 8D downstream the WT2, in which the open circles are obtained from the numerical simulation. The red lines present the results predicted by the proposed model and the blue solid lines show wake turbulence calculated by the IEC wake model with LSS principle as shown in Equation (9). The Root Mean Square Error of predicted turbulence intensity with respect to numerical results are also calculated for each case in Fig. 9, and the values are then normalized by ambient turbulence intensity I_a and summarized in Table 5. The proposed model well predicts the turbulence

Table 6
Maximum relative error of predicted power with respect to measurement data.

Model	Wind direction = **270**±**1**°	Wind direction = **222**±**1**°	Wind direction = **312**±**1**°
PARK model	38.6%	24.6%	24.8%
GH WindFarmer (modified PARK model)	25.1%	24.6%	24.8%
Proposed model	11.4%	4.4%	11.3%

distribution in the wake region with low RMSE, since the wake interaction induced turbulence is considered by the developed correction term in LSS principle. This is the case for both full overlap and partial overlap cases. However, the IEC wake model implemented with LSS principle gives conservative prediction in the near wake region for the full overlap wakes and large overestimation in the partial overlap wake regions, thus it shows significantly larger RMSE for all three cases. It is noticed that the predicted turbulence profiles still show some discrepancies with the numerical results especially for the case in Fig. 9c, which is due to the fact that the proposed correction term has some empirical factors and it is not expected to account for all phenomenon related with wake interaction.

To further evaluate the performance of the proposed model, the Horns Rev offshore wind farm is selected for validation, since it has been extensively studied and a dataset including Large Eddy Simulation (LES) results [29] and field measurement [30] are available for a benchmark. As shown in Fig. 10, this wind farm consists of 80 Vestas V-80 2 MW wind turbines arranged in a rhomboid shape with 10 columns in the East-West direction and 8 rows in the North-South direction. The distances between consecutive turbines are 7.0 D, 9.3 D, and 10.4 D for wind direction $\theta_{wind} = 270°$, 222° and 312°, respectively, where turbines are in a full overlap wake condition as noted by the solid arrows in Fig. 10a. The wind turbine has a rotor diameter of D = 80 m and a hub height of H = 70 m, and its thrust curve and power curve, which are used to evaluate the wake effects and power, are shown in Fig. 10b.

Fig. 11 shows a contour plot of the streamwise turbulence intensity on a horizontal plane at the hub height under the wind directions of 270° and 274°, which represents the case of full overlap and partial overlap wake condition, respectively. It is found that the flow pattern of the turbulent flow field predicted by the proposed multiple wake model favorably agrees with that simulated by LES turbulence model, in which the enhanced dual-peak in the full overlap condition and the weakened parts in the partial overlap areas are well reproduced.

For quantitative comparison, the streamwise turbulence intensity and mean velocity at the hub heigh, as well as the power production under wind direction of 270° predicted by the proposed model, the PARK model, as well as the modified PARK model are plotted together with the LES results [29] in Fig. 12. The PARK model, used in industry-standard software of WAsP [31]; is one of the most common analytical wake model for wind farms, which is based on the wake model by Jensen [32]; along with the Ambient-based Root Sum Square superposition approach suggested by Katic et al. [7]. The modified PARK model is the wake model used for wind farm layout optimization in the commercial software of GH WindFamer [33], the detail of which is described in Appendix A. For the PARK model and the modified PARK model as well, a constant linear wake growth rate of 0.04 for offshore application is used according to the suggestion in WAsP. In Fig. 12a, it is clearly shown that under the full overlap condition, the turbulence intensity increases significantly in the downstream and then reached an equilibrium value after two rows of wind turbines, and this is favorably reproduced by the proposed model. Note that in the PARK model as well as the modified PARK model, the turbine induced added turbulence is not modelled and the local turbulence is assumed to be the same as the ambient one, which significantly underestimates the turbulence intensity inside the wind farm. As a result shown in Fig. 12b and c, the PARK model with a constant wake growth tends to significantly underestimate the mean velocity and power output since the effects of increased turbulence level to wake recovery is not included. To overcome this drawback, the local wind speed experienced by the wind turbine is forced to be fully recovered to ambient wind speed in the modified PARK model, which leads to almost constant values of mean velocity and power for the downstream turbines but still under predict them. By contrast, the local added turbulence intensity on rotor is automatically considered for the prediction of velocity deficit in multiple wakes by the proposed model, thus a good agreement between the LES results and proposed model is found for both mean velocity and power production.

Fig. 13 shows the power production for three wind directions of 270°, 222°, and 312° with a 2° sector under the freestream wind speed of 8±0.5 m/s, in which open circles are field measurement data from SCADA [30], the blue dot-dashed lines and green dashed lines denote the power productions simulated by the PARK model and modified PARK model in GH WindFarmer, respectively, and red lines present the values predicted by the proposed multiple wake model. The maximum relative error of predicted power with respect to measured data is also estimated for each case and summarized in Table 6. The proposed model shows smallest error for each wind direction, since it provides favorable good agreement with the measurements of downstream turbines. However, the PARK model gives substantial underestimations with large errors. It is noticed that the maximum error predicted by PARK model generally occurs at the second row, which means that the main discrepancy derives from the original single wake model by Jensen [32]. Therefore, the modification done in GH WindFarmer could only achieve slight improvement after second row, while the accuracy in terms of the maximum relative error could not be improved, especially in the cases with the wind directions of 222° and 312°.

3.3. *Optimal wind sector width, wind speed bin and yaw offset limit for wake steering control*

In order to determine the optimal wind sector width and yaw offset limit for wake steering control, a case study is conducted with the new multiple wake model. The optimization framework is constructed in MATLAB and solved on a high-performance distributed computing system.

The wind speed and wind direction used as a basis for the optimization was measured by a cup anemometer and a wind vane installed on the met mast at 80 m height, which is located at a near-coastal site in Tomamae wind farm, Hokkaido of Japan [34]. The measurements consist of a one-year time series of 10-min average data during the period from November 1, 2015 to October 30, 2016 as shown in Fig. 14a. The wind rose is generated from these measurements and shown in Fig. 14b, in which the wind rose has a wind sector width of 5° and a wind speed bin of 1 m/s, and the west is found to be the prevailing wind direction. The wind speed

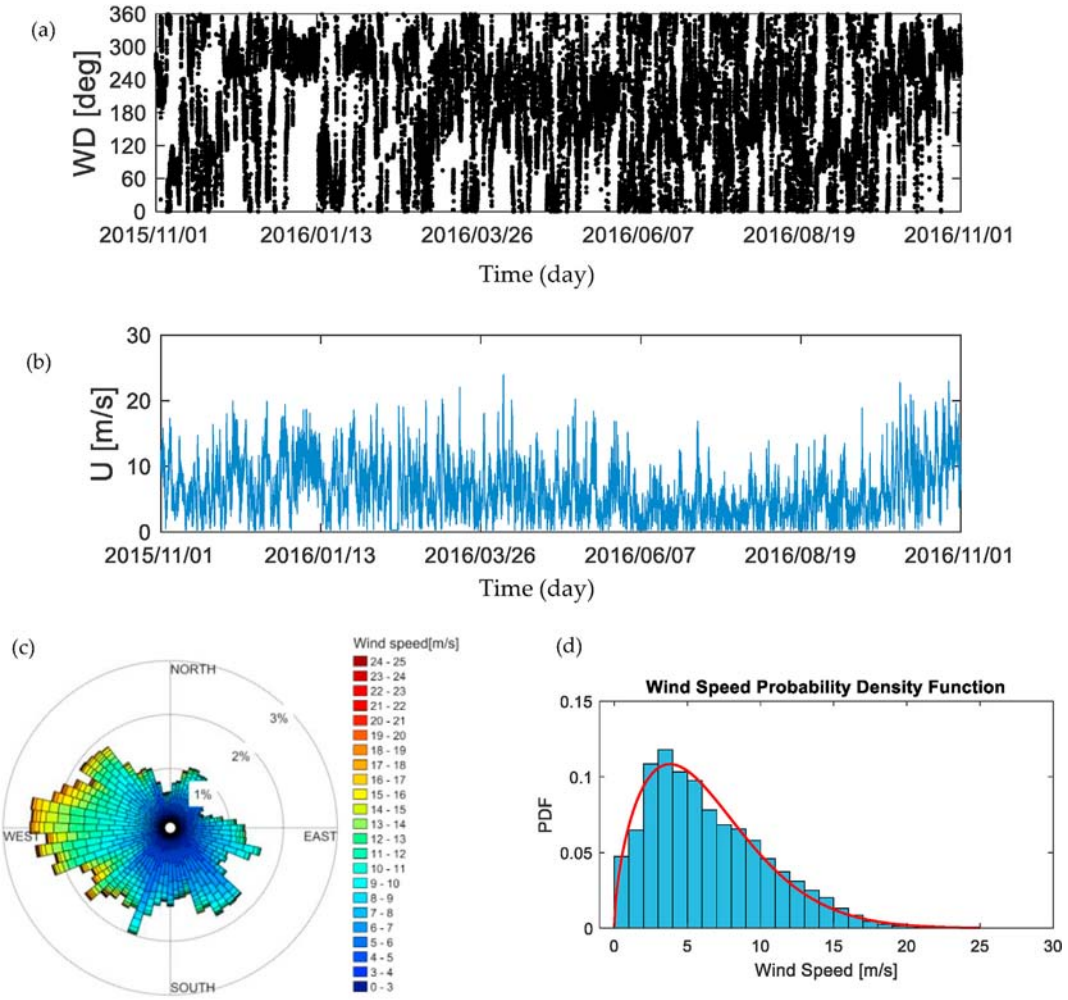

Fig. 14. Annual Wind condition used for wake steering optimization: time series of 10-min average (a) wind speed and (b) wind direction measured by a met mast in Tomamae wind farm, Japan during 2015/11/01 to 2016/10/31, (c) the generated wind rose, (d) frequency distribution of wind speed, where the red solid lines denotes the fitted Weibull distribution. (For interpretation of the references to colour in this figure legend, the reader is referred to the Web version of this article.)

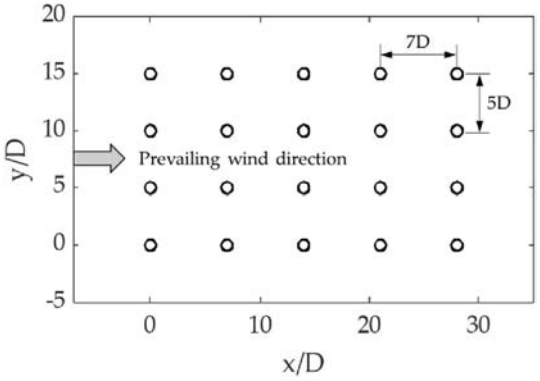

Fig. 15. Layout of a representative wind farm for power maximization through wake steering control, where the gray arrow denotes the prevailing wind direction.

distribution is analyzed and shown in Fig. 14c, where the probability density function is fitted by Weibull distribution with the mean speed of 6.5 m/s and k = 1.6. A representative wind farm is designed to consist of 20 wind turbines with 4 rows and 5 columns. Considering the typical distance of wind farm, the spacing of the turbines is set to 7D and 5D in the longitudinal and lateral distance, respectively. As shown in Fig. 15, to ensure a high energy efficiency, the wind turbines are arranged in a grid form that the longitudinal axis is set to along the prevailing wind direction, i.e. the west wind direction. The NREL 5-MW reference wind turbine is used to provide thrust coefficient and power as a function of wind speed and yaw angle as shown in Fig. 4.

Firstly, the wake steering optimization is performed for a discrete set of wind directions in the interval $[0°, 360°)$ binned at $1°$ and wind speeds between cut-in and cut-out $[3\ \mathrm{m/s}, 25\ \mathrm{m/s}]$ binned at 1 m/s. Fig. 16 shows one example of the flow field predicted by the proposed multiple wake model, under the wind speed of 8 m/s and the wind direction of $5°$, for both the baseline with greedy control and optimized operation with wake steering which results in a relative power gain of 8.2%. It can be clearly identified that the four column downstream turbines are originally partially waked under greedy control, and those wakes are redirected aside from the downstream turbines when the wake steering control is performed.

Subsequently, the generated optimal yaw offset angles are stored in 3 different levels of lookup table (LUT) with wind sector width of $1°$, $2°$ and $5°$ (noted as LUT-1deg, LUT-2deg, and LUT-5deg), where the wind speed bin width is kept 1 m/s. To investigate the sensitivity of wind sector width in the LUT-based

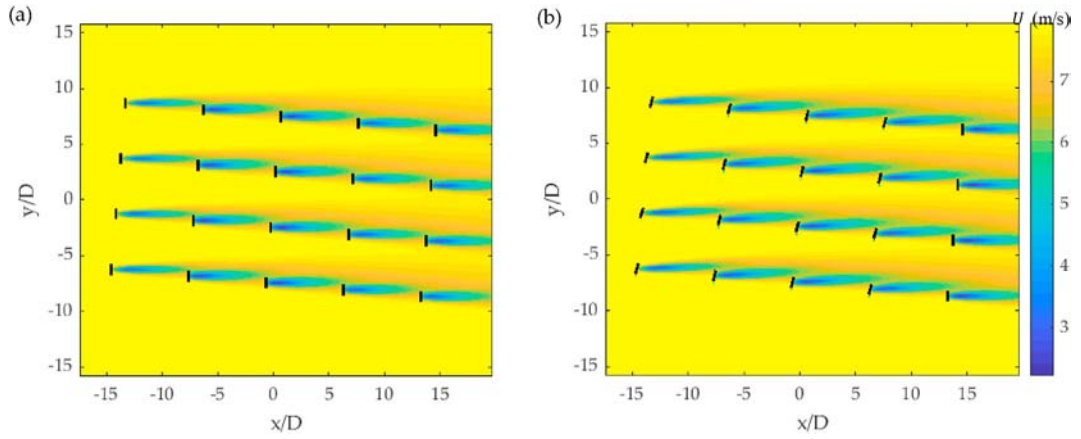

Fig. 16. Contours of wind speed in the wind farm at the hub height under the wind speed of 8 m/s and the wind direction of 5°: (a) baseline operation with greedy control and (b) optimized operation with wake steering control which results in a relative power gain of 8.2%.

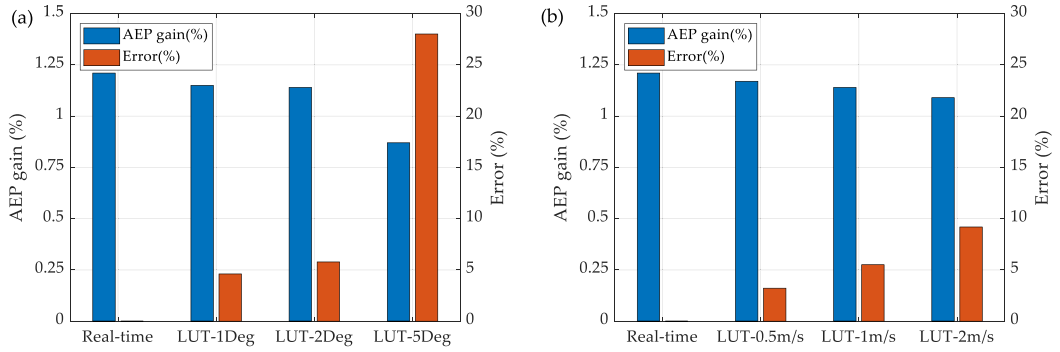

Fig. 17. AEP gains obtained using the real-time optimization and LUT-based optimization with (a) different wind sector widths and (b) wind speed bins. The wind speed bin is fixed to 1 m/s in (a) and the wind sector width used in (b) is 2°.

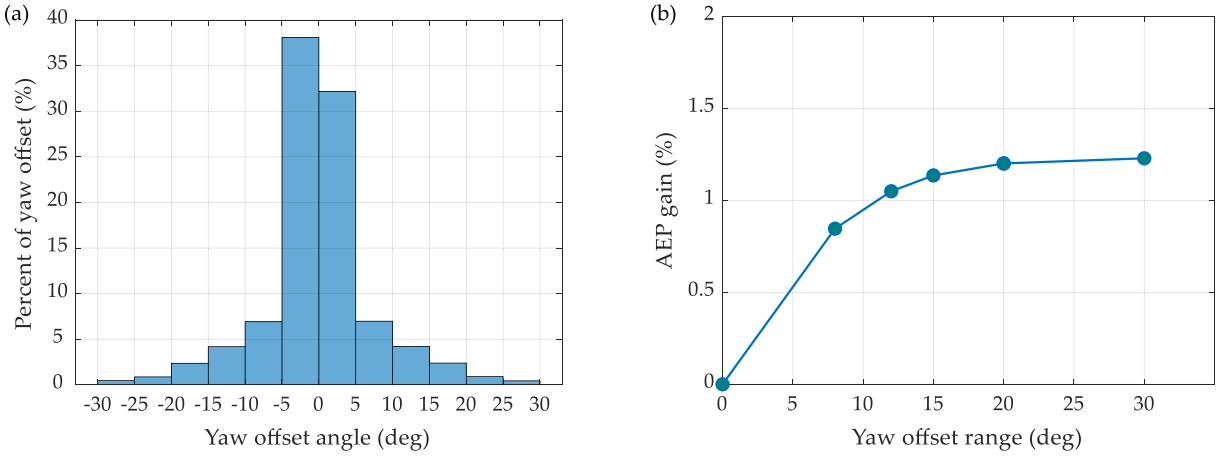

Fig. 18. Summary of LUT-based yaw optimization under different yaw offset limit: (a) percentage of yaw offset angles when the yaw limit of 30° is used; (b) AEP gains versus diferent yaw offset limits.

optimization, these three levels of LUT are utilized to estimate the AEP gain (%) separately, with one-year wind measurement data as shown in Fig. 14. The process described in Section 2.3 is used and the AEP gain is calculated as

$$\Delta AEP(\%) = \left(\frac{\sum_{i=1}^{N_T} \sum_{j=1}^{N_{10min}} P_i^{opt}(t_j)}{\sum_{i=1}^{N_T} \sum_{j=1}^{N_{10min}} P_i^{greedy}(t_j)} - 1 \right) \times 100\% \tag{19}$$

where, $P_i^{opt}(t_j)$ and $P_i^{greedy}(t_j)$ represent the power produced by turbine i at time j with optimized yaw offset and greedy control, respectively. In addition, the real-time optimization is also performed for comparison, and the AEP gains are summarized in Fig. 17a, where the relative error of ΔAEP_{LUT} produced by LUT with respect to that by real-time optimization ΔAEP_{RT} is evaluated as

$$\varepsilon_{LUT}(\%) = \frac{|\Delta AEP_{LUT} - \Delta AEP_{RT}|}{\Delta AEP_{RT}} \times 100\% \tag{20}$$

Comparing the AEP gain given by the real-time optimization, it is found that the LUT-5deg used in the previous studies presents a large error of 34.5%. By using the LUT-2deg, the relative error can be significantly reduced to 5.8%, and LUT-1deg gives quite close error to the one by LUT-2deg as shown in Fig. 17a. To further investigate the sensitivity of wind speed bin, three levels of lookup table (LUT) binned at 0.5 m/s, 1 m/s and 2 m/s (noted as LUT-0.5 m/s, LUT-1m/s, and LUT-2m/s) are also evaluated, where the wind sector width is fixed as 2°. When the wind speed bin is refined to 0.5 m/s, the result presents better agreement with that by real-time optimization with the smallest error fof 3.2%, which is almost half of that by LUT-1m/s as shown Fig. 17b. Therefore, it can be concluded that LUT with the wind sector width of 2° and wind speed bin of 0.5 m/s is acceptable for the engineering application of wake steering control.

Furthermore, to investigate that how much yaw offset limit is enough for the implementation, a series of yaw offset limits with values of ±8°, ±12°, ±15°, ±20°, ±25°, and ±30° are investigated for the wake steering control. The one-year wind measurement data as shown in Fig. 14 are used as the input and the LUT-2deg is adopted to perform the optimization. Firstly, the percentage distribution of optimized yaw offset angles obtained from all the cases (a total of 1051200 yaw offset points) with the yaw offset limit of ± 30° are analyzed and shown in Fig. 18a. It is noticed that the yaw offset of the turbines in most cases is smaller than 15°, which implies that the use of yaw offset larger than 15° would not have a high potential to provide greater power gain. To determinate the optimal yaw offset limit, the AEP gains estimated using different yaw offset limits are summarized in Fig. 18b. It is found that the yaw offset limit larger than 15° would only result in an additional AEP gain of up to 0.07%. On the other hand, a yaw offset larger than 15° increases the fatigue load of wind turbines. Following the safety requirement by IEC standard and the results shown in Fig. 18, the yaw offset limit of ±15° is recommended in the wake steering control for wind farm power maximization.

4. Conclusions

In this study, a systematic numerical simulation for multiple wakes of two wind turbines under the different wind directions is carried out by using the Reynolds Stress turbulence model. A new multiple wake model is developed based on the numerical investigation of wake interactions. The proposed model is then applied to wind farm power maximization by wake steering control. Following conclusions are obtained:

1. The characteristics of multiple wakes of two wind turbines under the representative condition of full overlap and partial overlap are systematically investigated. The mechanism of wake interaction and its effects on the turbulent flow filed are clarified by the numerical simulations.
2. A new multiple wake model accounting for the local turbulent flow field on the rotor is proposed, in which velocity deficits are combined by Linear Superposition, and turbulences are added using Linear Superposition of Square with a correction term to consider the wake interaction. The proposed model shows good agreement with the normalized power obtained from numerical simulations and field measurements, while the conventional Park model underestimates the turbine induced added turbulence and power production as well.
3. A maximization framework of wind farm power production by wake steering control is developed based on the new multiple wake model. The wind sector width of 2° with the wind speed bin of 0.5 m/s is proposed for the engineering application of lookup-table-based wake steering optimization, which reduces the prediction error of AEP gain from 34.5% to 3.2%. In addition, the yaw offset limit of ±15° is recommended to satisfy both the maximization of power production and the safety requirement of IEC standard.

Wake steering control is an active and growing field of research, while there are still some research gaps, such as fatigue load mitigation, filed validation and uncertainties concerning AEP gain.

Author contributions

This study was done by Guo-Wei Qian and Takeshi Ishihara. Guo-Wei Qian and Takeshi Ishihara designed the structure of the paper and wrote the paper.

Declaration of competing interest

The authors declare that they have no known competing financial interests or personal relationships that could have appeared to influence the work reported in this paper.

Acknowledgments

This research was carried out as a part of the project of Social Implementation of Artificial Intelligence Technology for Wind Turbines funded by NEDO. The authors express their deepest gratitude to the concerned parties for their assistance during this study.

Appendix A. Modified PARK model in GH WindFarmer

The modified PARK model in GH WindFarmer is based on the formula by Katic et al. [7]. This model assumes that the wake expands linearly behind the rotor and predicts the velocity deficit ΔU_i by a rectangular wind speed profile as

$$\Delta U_i = U_{i,0}\left(1 - \sqrt{1 - C_t}\right)\left(\frac{D}{D + 2kx}\right)^2 \tag{A.1}$$

where $U_{i,0}$ is the axial wind speed incident on the turbine, C_T is the thrust coefficient, D is the rotor diameter, x is the downstream distance from the rotor, k is the wake decay constant and is expressed as

$$k = \frac{A}{\ln(h/z_0)} \tag{A.2}$$

where A is a constant equal to 0.5, h is the hub height of turbine, and z_0 is the roughness length. It means that k is set the same value for all wind directions.

The turbine induced added turbulence is not considered in this model, which means that the local turbulence intensity $I_{i,0}$ incident on the turbine is taken as the ambient one.

$$I_{i,0} = I_a \tag{A.3}$$

To consider the wake effects of upstream wind turbines on a downstream turbine, two assumptions are taken: (1) the incident wind speed on each turbine $U_{i,0}$ is corrected to ambient wind speed U_0 to calculate the individual velocity deficit by Equation (A1); (2) the overall wake effect is taken as the largest wind speed deficit and the flow filed in the wake flow of multiple turbines are subsequently calculated as

$$U_w = U_0 - \max(\Delta U_1, \ldots, \Delta U_i \ldots, \Delta U_n) \quad (A.4)$$

References

[1] Kheirabadi AC, Nagamune R. A quantitative review of wind farm control with the objective of wind farm power maximization. J Wind Eng Ind Aerod 2019;192:45–73. https://doi.org/10.1016/j.jweia.2019.06.015.

[2] van Wingerden JW, Fleming PA, Göçmen T, Eguinoa I, Doekemeijer BM, Dykes K, Lawson M, Simley E, King J, Astrain D, Iribas M. Expert elicitation on wind farm control. J Phys Conf 2020;1618:22025. https://doi.org/10.1088/1742-6596/1618/2/022025.

[3] Giebel G, Göçmen T, Van Wingerden JW, Fleming PA, King J. State of the art and research gaps in wind farm control-Results of a recent workshop, in: WindEurope Offshore 2019: our Energy. Our Future: How Offshore Wind Will Help Europe Go Carbon Neutral; 2019. p. 1. https://doi.org/10.5194/wes-2-229-2017.

[4] Fleming PA, Ning A, Gebraad PMO, Dykes K. Wind plant system engineering through optimization of layout and yaw control. Wind Energy 2016;19:329–44. https://doi.org/10.1002/we.1836.

[5] Gebraad P, Thomas JJ, Ning A, Fleming P, Dykes K. Maximization of the annual energy production of wind power plants by optimization of layout and yaw-based wake control. Wind Energy 2016;20(1):97–107. https://doi.org/10.1002/we.1993.

[6] van Dijk MT, van Wingerden JW, Ashuri T, Li Y. Wind farm multi-objective wake redirection for optimizing power production and loads. Energy 2017;121:561–9. https://doi.org/10.1016/j.energy.2017.01.051.

[7] Katic I, Hojstrup J, Jensen NO. A simple model for cluster efficiency i.katic.j.højstrup. n.o.jensen. Eur. Wind energy Assoc. Conf. Exhib 1986;1986:407–10.

[8] Niayifar A, Porté-Agel F. Analytical modeling of wind farms: a new approach for power prediction. Energies 2016;9(741). https://doi.org/10.3390/en9090741.

[9] P.B. Lissaman S. Energy effectiveness of arbitrary arrays of wind turbines J Energy 1979;3:323–8. https://doi.org/10.2514/3.62441.

[10] Zong H, Porté-Agel F. A momentum-conserving wake superposition method for wind farm power prediction. J Fluid Mech 2020;889. https://doi.org/10.1017/jfm.2020.77.

[11] Ishihara T, Qian GW. A new Gaussian-based analytical wake model for wind turbines considering ambient turbulence intensities and thrust coefficient effects. J Wind Eng Ind Aerod 2018;177:275–92. https://doi.org/10.1016/j.jweia.2018.04.010.

[12] Lin M, Porté-Agel F. Large-eddy simulation of yawed wind-turbine wakes: comparisons with wind tunnel measurements and analytical wake models. Energies 2019;12(4574). https://doi.org/10.3390/en12234574.

[13] Gebraad PMO, Teeuwisse FW, van Wingerden JW, Fleming PA, Ruben SD, Marden JR, Pao LY. Wind plant power optimization through yaw control using a parametric model for wake effects-a CFD simulation study. Wind Energy 2014;19(1):95–114. https://doi.org/10.1002/we.1822.

[14] Munters W, Meyers J. Dynamic strategies for yaw and induction control of wind farms based on large-eddy simulation and optimization. Energies 2018;11(177). https://doi.org/10.3390/en11010177.

[15] Fleming P, Annoni J, Shah JJ, Wang L, Ananthan S, Zhang Z, Hutchings K, Wang P, Chen W, Chen L. Field test of wake steering at an offshore wind farm. Wind Energy Sci. 2017;2:229–39. https://doi.org/10.5194/wes-2-229-2017.

[16] Fleming P, King J, Dykes K, Simley E, Roadman J, Scholbrock A, Murphy P, Lundquist JK, Moriarty P, Fleming K, van Dam J, Bay C, Mudafort R, Lopez H, Skopek J, Scott M, Ryan B, Guernsey C, Brake D. Initial results from a field campaign of wake steering applied at a commercial wind farm – Part 1. Wind Energy Sci. 2019;4:273–85. https://doi.org/10.5194/wes-4-273-2019.

[17] Fleming P, King J, Simley E, Roadman J, Scholbrock A, Murphy P, Bay C. Continued results from a field campaign of wake steering applied at a commercial wind farm: Part 2. Wind Energy Science Discussions; 2020. p. 1–24.

[18] IEC 61400-1. Wind energy generation systems - Part 1: design requirements, international electrotechnical commission. 2019.

[19] Cabezón D, Migoya E, Crespo A. Comparison of turbulence models for the computational fluid dynamics simulation of wind turbine wakes in the atmospheric boundary layer. Wind Energy 2011;14:909–21. https://doi.org/10.1002/we.516.

[20] Qian GW, Ishihara T. A new analytical wake model for yawed wind turbines. Energies 2018;11(665). https://doi.org/10.3390/en11030665.

[21] Ansys Inc. Fluent Theory Guide. Canonsburg, PA. 2015.

[22] Ferziger JH, Peric M. Computational methods for fluid dynamics. Springer; 2002.

[23] Burton T, Sharpe D, Jenkins N, Bossanyi E. Wind energy handbook. second ed. Wiley; 2011.

[24] Fluent Inc. Gambit 2.4 users Guide. 2006.

[25] Brugger P, Debnath M, Scholbrock A, Fleming P, Moriarty P, Simley E, Jager D, Murphy M, Zong H, Porté-Agel F. Lidar measurements of yawed wind turbine wakes: characterisation and validation of analytical models. Wind Energy Science Discussions; 2020. p. 1–31. https://doi.org/10.5194/wes-2020-73.

[26] Porté-Agel F, Bastankhah M, Shamsoddin S. Wind-turbine and wind-farm flows: a Review. Boundary-Layer Meteorol 2019;174:1–59. https://doi.org/10.1007/s10546-019-00473-0.

[27] Jonkman JM, Buhl ML. FAST user's Guide. 2005.

[28] MathWorks Inc. MATLAB 2019b. 2019.

[29] Wu YT, Porté-Agel F. Modeling turbine wakes and power losses within a wind farm using LES: an application to the Horns Rev offshore wind farm. Renew Energy 2015;75:945–55. https://doi.org/10.1016/j.renene.2014.06.019.

[30] Barthelmie RJ, Rathmann O, Frandsen ST, Hansen KS, Politis E, Prospathopoulos J, Neubert A. Modelling and measurements of wakes in large wind farms. J Phys Conf 2007;75–1:p012049 [IOP Publishing].

[31] Mortensen NG, Landberg L, Troen I, Petersen EL. Wind atlas analysis and application program (WAsP). Roskilde, Denmark: Riso National Laboratory; 1993.

[32] Jensen NO. A note on wind turbine interaction. Technical report. Roskilde, Denmark: Risø-M-2411, Risoe National Labo- ratory; 1983.

[33] WindFarmer GH. Wind farm design software: theory manual. Garrad Hassan and Partners Ltd. 2014.

[34] Qian GW, Ishihara T. Numerical study of wind turbine wakes over escarpments by a modified delayed detached eddy simulation. J Wind Eng Ind Aerod 2019;191:41–53. https://doi.org/10.1016/j.jweia.2019.05.004.

[35] Voutsinas S, Rados K, Zervos A. On the analysis of wake effects in wind parks. Wind Eng 1990:204–19.